Perspective

Israel Journal of Chemistry
www.ijc.wiley-vch.de

doi.org/10.1002/ijch.202300058

The Driven Liouville von Neumann Approach to Electron Dynamics in Open Quantum Systems

Oded Hod*[a] and Leeor Kronik*[b]

In honor of the 80th birthday of Prof. Helmut Schwarz, whose admirable scientific work and academic contributions continue to inspire us and many others.

Abstract: The driven Liouville von Neumann approach is a method to computationally explore electron dynamics and transport in nanoscale systems. It does so by imposing open boundary conditions on finite atomistic model systems, which drive them out of equilibrium. The approach is compatible with any underlying electronic structure treatment that can be phrased in terms of a single-particle framework, ranging from simple tight-binding descriptions to state-of-the-art density functional theory treatments of the interacting system. In this perspective, we motivate the approach, discuss its theoretical foundations, explain its essential elements, overview recent extensions and applications, and present remaining challenges and opportunities.

Introduction

The utilization of individual molecules as miniature electronic components was first envisioned in a seminal paper by Aviram and Ratner.[1] Since then, the invention of breakthrough technologies for the visualization and manipulation of systems at the atomic and molecular levels advanced this prediction towards realization.[2–11] Gaining control over the electron charge and spin degrees of freedom in such systems may further give rise to novel functionalities based on quantum mechanical phenomena, thus potentially redefining electronics and computation.[2,12–15] This, however, requires deep understanding of non-equilibrium dynamic and thermodynamic behavior of nanostructures coupled to their immediate surroundings and to the remote environment.[16–21] Notably, the miniature nature of molecular-based systems allows for a unique interplay between the availability of high resolution experimental data and accurate theoretical and computational treatments of electron and spin transport. Therefore, theory and computation play a prominent role in gaining physical insights into fundamental transport mechanisms, interpreting experimental observations, predicting new physical phenomena, and designing novel electronic and spintronic components for quantum information processing at the molecular level.

Early advances towards a non-equilibrium description of electronic systems coupled to external heat and particle reservoirs involved steady-state descriptions of transport phenomena. The most powerful and widely used approach in this context is the Landauer formalism,[22,23] which relates the conductance of a given molecular system to the probability of an electron to transmit through the molecule.[24–27] When applied with advanced non-equilibrium Green functions (NEGF)[7,24,27,28] techniques to evaluate the transmittance probability spectrum, a high level treatment of molecular junctions is attained, with possible consideration of inelastic scattering and strong correlation effects.[29–34] Many practical NEGF applications rely on an underlying description of the electronic structure that is obtained from density functional theory (DFT).[35] Within this approach, often referred to as NEGF-DFT, single particle Kohn-Sham (KS) molecular orbitals (MOs) are obtained self-consistently under an external bias,[36–43] thus taking into account its influence on the electronic structure of the molecular device. The results obtained using NEGF-DFT based calculations often provide qualitative understanding of the physical features appearing in molecular electronic measurements. Nevertheless, quantitative discrepancies between the predicted currents and experimental results may exceed an order of magnitude.[44] Apart from experimental uncertainties, these discrepancies reflect technical theoretical issues, such as poor understanding of the detailed atomic structure and structural dynamics

[a] *O. Hod*
Department of Physical Chemistry, School of Chemistry and The Sackler Centre for Computational Molecular and Materials Science, The Raymond and Beverly Sackler Faculty of Exact Sciences, Tel Aviv University, Tel Aviv 6997801, Israel
E-mail: odedhod@tauex.tau.ac.il
[b] *L. Kronik*
Department of Molecular Chemistry and Materials Science, Weizmann Institute of Science, Rehovoth 7610001, Israel
E-mail: leeor.kronik@weizmann.ac.il

Israel Journal of Chemistry

of the molecular junction;[45,46] formal issues relating to the fact that NEGF-DFT hybridizes a non-equilibrium formalism with a ground state electronic structure theory;[39,47,48] and perhaps above all that the underlying KS-DFT approach involves approximations that may considerably influence the outcome of the calculations.[44,49] Indeed NEGF calculations utilizing more advanced or beyond DFT approximations have been successful in improving quantitative accuracy.[45,50]

Going beyond steady-state descriptions, a formally exact framework for treating excited state electron dynamics is provided by explicit time-dependent methods, notably time-dependent Green's function approaches or time dependent (current) density functional theory (TD(C)DFT). Indeed, many important advances in adapting such tools to the problem of electron transport have been made.[51–93] The difficulty is that the former may be prohibitively expensive for routine use, whereas the latter requires care when implementing the open boundary conditions. This naturally bring us to the quest for a computationally expedient, yet sufficiently accurate and physically sound, treatment of open boundary conditions in TDDFT, or for that matter any underlying electronic structure treatment that can be phrased in terms of a single-particle framework. This would include a wide range of methods, from tight-binding and (semi−)empirical descriptions, through other mean-field treatments, to many-body perturbation theory and TDDFT itself.[94] The salient issue is that standard electronic structure approaches are intrinsically designed to treat either isolated systems or infinitely periodic structures. This enables the description of both ground state properties and excited state dynamics in such systems, which is important for understanding their structural, electronic, and optical response characteristics. However, electronic transport phenomena require the description of a finite system coupled to external reservoirs. If the latter are at different equilibrium states, non-equilibrium charge transport through the finite system will occur.

Perhaps the simplest approach to tackling this issue is to circumvent it, namely, to rely on discharge dynamics in a finite system as a means of exploring some aspects of transport through the open system. The general scheme involves a finite model system that is prepared in a polar state using, e. g., an external electric field, and running the dynamics from this initial state in the absence of the polarizing field. For a sufficiently large model system, the resulting charge oscillations may exhibit a quasi-steady-state current that mimics the true steady-state of the corresponding open system.[55,57,95,96] This quasi-steady state is, however, limited in duration and is eventually suppressed by reflections from the finite model system edges. Therefore, using discharge dynamics to study open quantum system behavior is applicable only at short timescales and true steady state can never be reached.

One remedy to the above problem is to use cyclic boundary conditions with a single lead setup.[47,97–99] Here, electrons that exit the simulation box on one side re-enter it at the other side. The external field thus accelerates the circulating electrons, which requires the introduction of a deceleration term to avoid unrealistic buildup of velocities. This can be achieved by, e. g., introducing a quantum master equation with a dissipative term that simulates the effect of electron-phonon interactions. Importantly, this approach provides a true steady-state and is not affected by unphysical reflections from the boundaries of a finite model system. However, computational demands dictate the use of relatively small lead models and thus the temperature of the phonon bath and the coupling strength used in the master equation have to be tuned to unphysically large values to obtain physically meaningful transport results.[100]

An alternative approach is to employ a two-lead setup and use imaginary potentials to absorb the accelerated charges when reaching the edges of the system, hence simulating irreversible charge flow into the leads.[51,52,101–109] Here, the main difficulty is the absence of charge conservation, limiting again the simulation to short time-scales, where charge depletion at the system boundaries does not significantly affect the transport dynamics at its center. This limitation has been overcome by introducing injection terms within a quantum master equation formulation that continuously drive the lead regions towards an appropriate equilibrium state.[110–112] However, the approach was shown in some cases to produce unphysical state populations.[113] Nonetheless, its intuitive and simple nature has triggered further efforts towards resolving the remaining difficulties and generalizing the methodology. One such approach, known as the driven Liouville von Neumann (DLvN) formalism, has emerged in recent years. In this Perspective, we explain the method, describe its current status, and provide an outlook for its future development.

The Driven Liouville von Neumann Formalism

The starting point of the DLvN approach is the commonly used formal partition of a molecular junction into three sections: the left and right leads and an extended molecule section consisting of the active molecule augmented by its adjacent lead sections – see Figure 1(left). The role of the lead sections in the extended molecule is to create spatial separation between the molecule of interest (including its chemical contacts to the leads) and the remote edges of the finite model system, where coupling to external reservoirs is implemented. This separation allows us to retain a physically and chemically realistic description of the molecule, including its coupling to the lead, that is unaffected by the choice of model used to mimic an open system.

The leads should serve to absorb any electron traveling from the active molecule towards the reservoirs. This can be achieved by introducing imaginary absorbing potentials to the Hamiltonian of the lead models. A simple choice for such a potential is to absorb all outgoing electrons at the same rate, Γ, regardless of their energy. Given that this absorption

Israel Journal of Chemistry

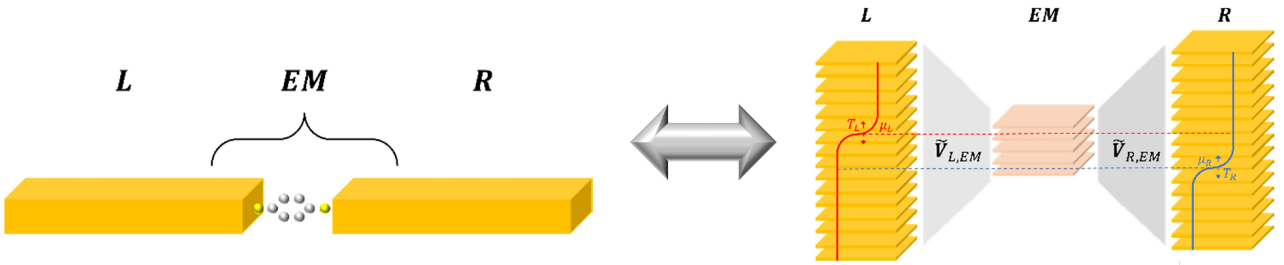

Figure 1. Illustration of the site-to-state transformation. Left: site representation of a molecular junction composed of left (L) and right (R) leads bridged by a (benzene dithiol) molecule. The extended molecule (EM) section includes the molecule, dressed by buffer lead model sections. Right: state representation of a molecular junction, where the L and R lead level manifolds are coupled to the single-particle states of the EM sections via the $\tilde{V}_{L/R,EM}$ coupling matrices. The Fermi-Dirac equilibrium state occupations of the L and R reservoirs, with chemical potentials $\mu_{L/R}$ and electronic temperatures $T_{L/R}$ are illustrated in red and blue, respectively.

represents broadening of the lead energy levels (due to their coupling to implicit reservoirs), the choice of an energy-independent Γ is reasonable if there are no strong variations in the density of states of the leads in the vicinity of the Fermi energy. The implementation of such an absorbing potential therefore requires a transformation from the spatial representation of the junction to an energy picture – see Figure 1(right). To this end, consider the single-particle Hamiltonian matrix representation of the entire finite model system within some localized orthogonal basis-set representation, referred to as the site representation:

$$H = \begin{pmatrix} H_L & V_{L,EM} & 0 \\ V_{EM,L} & H_{EM} & V_{EM,R} \\ 0 & V_{R,EM} & H_R \end{pmatrix}, \tag{1}$$

where H_i are Hamiltonian block matrix representations of the $i = L, EM, R$ sections, $V_{i,j}$ are the corresponding inter-section coupling blocks, and the EM section is assumed to be sufficiently large, such that the direct coupling between the L and R blocks is negligible.

The transformation from this representation to an energy based one (henceforth referred to as the state representation) proceeds by first diagonalizing separately each of the H_i blocks, using appropriate unitary matrices U_i:

$$\tilde{H}_i = U_i^{\dagger} H_i U_i, \tag{2}$$

and defining the so-called site-to-state block diagonal transformation matrix as:[114]

$$U = \begin{pmatrix} U_L & 0 & 0 \\ 0 & U_{EM} & 0 \\ 0 & 0 & U_R \end{pmatrix}. \tag{3}$$

Applying the transformation U to the full Hamiltonian matrix H yields:

$$\tilde{H} = U^{\dagger} H U = \begin{pmatrix} \tilde{H}_L & \tilde{V}_{L,EM} & 0 \\ \tilde{V}_{EM,L} & \tilde{H}_{EM} & \tilde{V}_{EM,R} \\ 0 & \tilde{V}_{R,EM} & \tilde{H}_R \end{pmatrix}, \tag{4}$$

where the diagonal blocks, $\tilde{H}_i$, are diagonal matrices containing the energies of the eigenstates of the i^{th} section, and the off-diagonal blocks $\tilde{V}_{ij} = U_i^{\dagger} V_{ij} U_j$ contain the coupling matrix elements between all eigenstates of sections i and j – see Figure 1(right). We note that the site-to-state transformation can be used to study the coupling scheme between an adsorbent molecule and a surface, including the effects of level shifting and broadening and their influence on the electronic structure and transport properties of the molecule.[115,116]

In the state representation, the single-particle reduced density matrix, $\tilde{P}$, obeys the following matrix form of the Liouville von Neumann (LvN) equation of motion (EOM):

$$\frac{d\tilde{P}}{dt} = -\frac{i}{\hbar}[\tilde{H}, \tilde{P}], \tag{5}$$

where $i = \sqrt{-1}$ and $\hbar = h/2\pi$ is the reduced Planck constant. Applying an energy-independent absorbing potential to all eigenstates of the L and R sections amounts to adding the following term to $\tilde{H}$ of Eq. (4):

$$\tilde{V}^{abs} = -\frac{i\hbar}{2}\Gamma \begin{pmatrix} I_L & 0 & 0 \\ 0 & 0 & 0 \\ 0 & 0 & I_R \end{pmatrix}, \tag{6}$$

and replacing $\tilde{H}$ by $\tilde{H} + \tilde{V}^{abs}$ in the Liouville von-Neumann Eq. (5), to obtain:

$$\frac{d\tilde{P}(t)}{dt} = -\frac{i}{\hbar}\left[\tilde{H},\tilde{P}(t)\right] - \Gamma\begin{pmatrix} \tilde{P}_L(t) & \frac{1}{2}\tilde{P}_{L,EM}(t) & \tilde{P}_{L,R}(t) \\ \frac{1}{2}\tilde{P}_{EM,L}(t) & 0 & \frac{1}{2}\tilde{P}_{EM,R}(t) \\ \tilde{P}_{R,L}(t) & \frac{1}{2}\tilde{P}_{R,EM}(t) & \tilde{P}_R(t) \end{pmatrix}. \quad (7)$$

Eq. (7) describes the dynamics of a system in which electrons traveling from the *EM* region into the *L* or *R* sections are absorbed (represented by decaying diagonal elements of the density matrix), with the corresponding coherence terms (off-diagonal density matrix elements) decaying commensurately. Notably, the dynamics of the *EM* density matrix block are not explicitly affected by the non-unitary term in Eq. (7) – note the central zero block.

To describe electrons injected into the system, recall that they should carry the equilibrium Fermi-Dirac distribution of the corresponding bath, to which the lead (implicitly) connects. This is achieved by adding the following injection term to Eq. (7):

$$\Gamma\begin{pmatrix} \tilde{P}^0_L & 0 & 0 \\ 0 & 0 & 0 \\ 0 & 0 & \tilde{P}^0_R \end{pmatrix}, \quad (8)$$

where $\tilde{P}^0_{L/R}$ are diagonal matrices of the dimensions of the left/right lead models, the elements of which are given by the Fermi-Dirac distribution of the corresponding lead state occupations: $\left[\tilde{P}^0_{L/R}\right]_{ij} = \delta_{ij}\left[e^{\left(\varepsilon_{L/R_i}-\mu_{L/R}\right)/\left(k_B T_{L/R}\right)}+1\right]^{-1}$, $\{\varepsilon_{L/R}\}$ are the eigenenergies, $T_{L/R}$ are the electronic temperatures of the left/right leads, and the lead chemical potentials are given by $\mu_{L/R} = E_F \pm 0.5|e|V_b$, where E_F is usually set to the Fermi energy of the entire finite model system, e is the electron charge, and V_b is the bias voltage. Importantly, the electron injection rate is chosen to be identical to the corresponding absorption rate to assure the eventual emergence of a steady-state. The final form of the DLvN EOM therefore reads as follows:

$$\frac{d\tilde{P}(t)}{dt} = -\frac{i}{\hbar}\left[\tilde{H},\tilde{P}(t)\right] - \Gamma\begin{pmatrix} \tilde{P}_L(t)-\tilde{P}^0_L & \frac{1}{2}\tilde{P}_{L,EM}(t) & \tilde{P}_{L,R}(t) \\ \frac{1}{2}\tilde{P}_{EM,L}(t) & 0 & \frac{1}{2}\tilde{P}_{EM,R}(t) \\ \tilde{P}_{R,L}(t) & \frac{1}{2}\tilde{P}_{R,EM}(t) & \tilde{P}_R(t)-\tilde{P}^0_R \end{pmatrix}. \quad (9)$$

Going beyond the heuristic derivation provided above,[114] the DLvN EOM was formally derived from non-equilibrium Green's function theory by further assuming that the relaxation dynamics of the explicit lead levels is independent of the presence of the molecule and that any time dependence in the leads (e.g., time-dependent bias voltages) can be considered adiabatic.[117] Furthermore, Eq. (9) can be recast in Lindblad form, thus justifying the complete positiveness of the propagated single-particle density matrix.[118]

By propagation of Eq. (9), bond current dynamics can be obtained from the corresponding off-diagonal density matrix element.[114] This was recently demonstrated for an oligo-(phenylene-ethynylene)-graphene nanoribbon junction model, where the time- and spatially-resolved electron dynamics unraveled insightful mechanistic details on time scales ranging from atto- to pico-seconds.[119]

Note that when deriving Eq. (9), we introduced the driving rate, Γ, as a free parameter. Its effect on the current dynamics can be demonstrated by considering the simple tight-binding chain junction model of Figure 2a.[114] Starting from lead density matrix blocks of $\tilde{P}_{L/R}(t) = \tilde{P}^0_{L/R}$ and a diagonal *EM* density matrix block populated up to the Fermi energy of the full finite model system, the current dynamics at the middle of the *EM* section under a bias voltage of 0.3 V is plotted in Figure 2b for several Γ values. For $\Gamma = 0$ discharge dynamics is obtained, i.e. no stable steady-state is reached and instead the charge oscillates between the finite lead models. However, if the lead model size is chosen to be sufficiently large (which is the case here) a quasi-steady-state current develops, the value of which matches that obtained using the Landauer formalism (brown × mark). Increasing the value of Γ dampens the current oscillations, eventually achieving a stable steady-state. Notably, the value of the steady-state current matches well the Landauer value and is found to be quite insensitive to the choice of driving rate over nearly three decades of Γ. Only when the driving rate is too large do deviations ensue from the correct steady-state current, as discussed in more detail below. The inset of Figure 2b presents the steady-state level occupations of the three system sections, demonstrating that the lead occupations correctly follow the corresponding bath Fermi-Dirac distributions with some minor deviations within the Fermi transport window, due to finite size effects. The *EM* occupations demonstrate the expected gradual population decrease with increasing lead level energy, which is found to be insensitive to the lead model size. Figure 2c presents the current dynamics obtained under several bias voltages, clearly demonstrating that the obtained steady-state values match the Landauer I–V curve (inset of Figure 2c).

Extensions and Applications

Having demonstrated the basic utility of the DLvN approach within the context of a simple tight-binding model, we now discuss various extensions of the methodology and their usage in various practical applications. First of all, Eq. (9) above was derived for an orthonormal atomic-centered basis-set representation of the density matrix. The DLvN EOM can

Israel Journal of Chemistry

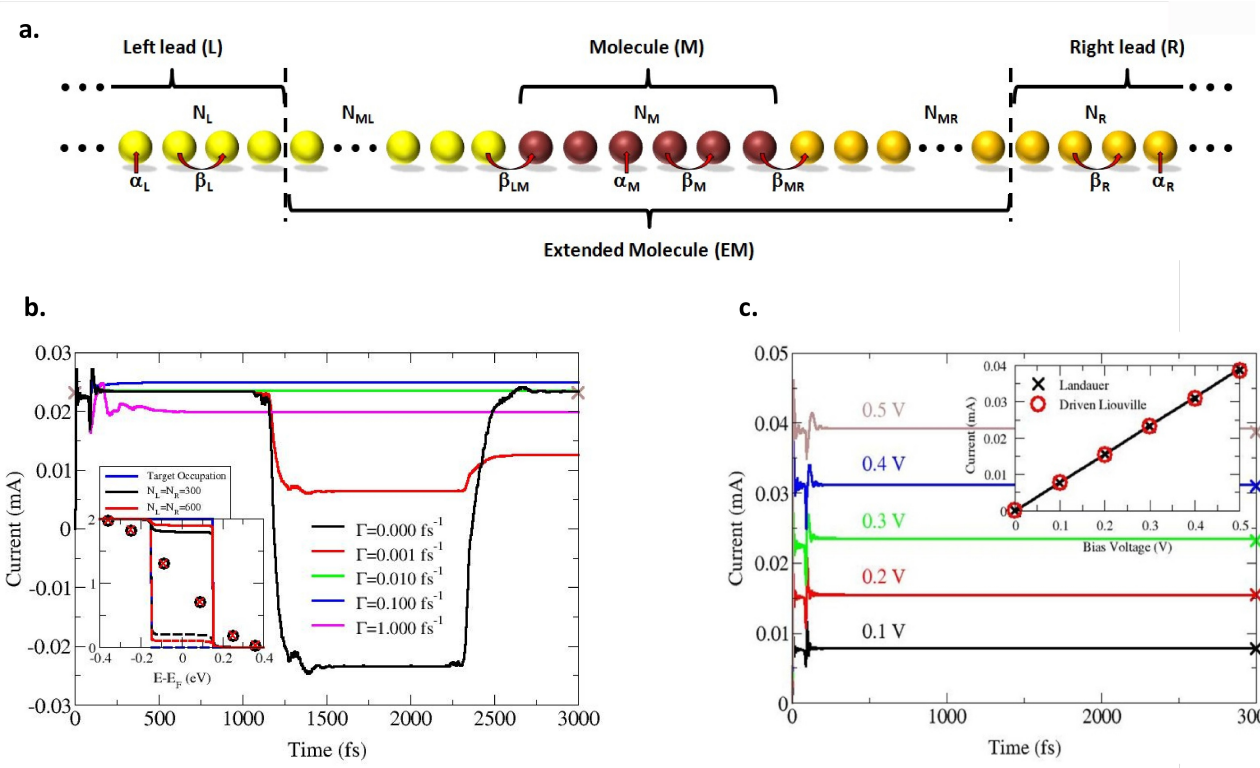

Figure 2. Tight-binding chain junction model simulations. (a) Schematic representation of the tight-binding two-lead chain model. Yellow, maroon, and orange spheres represent the left lead, molecule, and right lead, respectively. The extended molecule region is marked explicitly. α_L, α_M, α_R, β_L, β_M, and β_R mark the onsite energies (α) and hopping integrals (β) of the left lead (L), molecule (M), and right lead (R) subsystems, respectively. β_{LM} and β_{MR} are the coupling matrix elements between the left lead and the molecule and between the molecule and the right lead, respectively. N_L, N_M, and N_R are the number of sites used to represent the left lead, molecule, and right lead models, respectively. N_{ML} and N_{MR} are the number of extended molecule atoms belonging to the left and right leads, respectively; (b) Effect of the driving rate (Γ) on the time-dependent current under a bias voltage of $V_b = 0.3$ V and reservoir electronic temperatures of 0 K, for a tight-binding chain consisting of $N_L = N_R = 300$, $N_{ML} = N_{MR} = 50$, and $N_M = 6$, with on-site energies of 0 eV, and hopping integrals of -0.2 eV. The black curve was obtained using the microcanonical approach ($\Gamma = 0$) in the state representation. The red, green, blue, and purple curves were obtained using $\Gamma = 0.001$, 0.01, 0.1, and 1.0 fs^{-1}, respectively. The brown X mark represents the Landauer steady-state currents. Inset: left lead (full lines), right lead (dashed lines), and molecule (symbols) steady-state occupations obtained using lead models of $N_L = N_R = 300$ (black) and $N_L = N_R = 600$ (red) compared to the corresponding target lead-equilibrium step-function distributions (blue); (c) Time-dependent current calculated at various bias voltages using a driving rate of $\Gamma = 0.01$ fs^{-1}. Colored X marks designate the corresponding Landauer steady-state currents. Inset: current vs. bias curve calculated from the steady-state currents obtained at a simulation time of 3 ps (red circles) and the Landauer formalism (black X marks). Adapted with permission from Ref. [114].

be generalized to accommodate for non-orthogonal basis-set representations, which are often used in practical quantum chemistry applications.[120] In that case, the overlap matrix that appears in the site representation of the EOM possesses non-zero overlaps between different system sections. These can be eliminated by a non-unitary block-diagonalization transformation that rotates the basis functions of the EM section to be orthonormal to those of the lead sections, leaving only diagonal overlap blocks, S_i, where again $i = L, EM, R$.[121] Following this, the site-to-state transformation proceeds as above, with the only difference being that a generalized eigenvalue problem, rather than a standard one, is solved separately for each block, such that the transformation matrix blocks (see Eq. (2)) obey $U_i^{\dagger} S_i U_i = I_i$. Using this approach, the utility of the DLvN-EOM was demonstrated for non-orthogonal extended Hückel Hamiltonian descriptions. This allowed to uncover unique transport phenomena, e. g. the fact that consecutive molecular states may possess radically different dynamic and steady-state occupations depending on the nature of the corresponding molecular orbital and its relative coupling to the source and the sink electrodes (see Figure 3).[115,120]

While the non-orthogonal representation enables the exploration of realistic (rather than phenomenological) molecular junction models, the generalized DLvN equation of motion remains Markovian in nature. This seemingly contradicts the standard notion that reduced system representations introduce memory terms to the dynamics.[122] However, the validity of the Markovian approximation within the DLvN approach stems from the fact that one introduces

Israel Journal of Chemistry

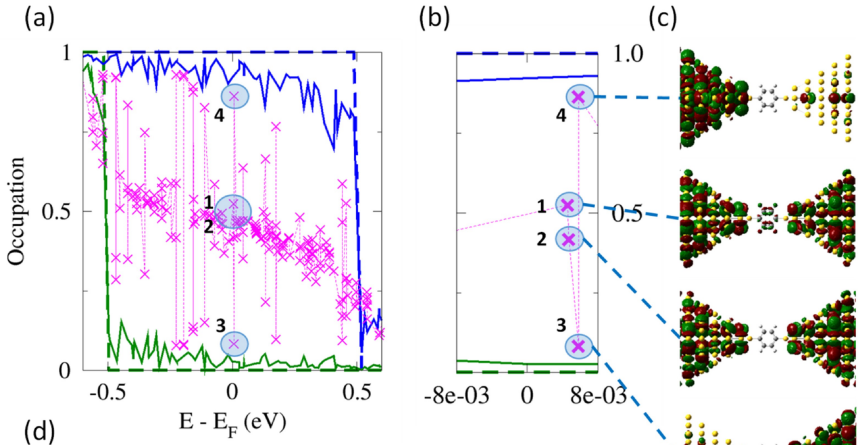

(d)

Number of State	Steady State Occupations	Effective Coupling to the Left Lead (eV)	Effective Coupling to the Right Lead (eV)
1	0.500	0.0038	0.0029
2	0.420	0.0034	0.0042
3	0.083	0.0007	0.0118
4	0.860	0.0117	0.0007

Figure 3. Steady-state single-particle state occupations of different benzene-dithiol junction sections. (a) Left lead (solid blue line), right lead (solid green line) and extended-molecule (magenta × marks) steady-state occupations, compared to the corresponding target lead-equilibrium step-function distributions (blue and green dashed lines, respectively). (b) Zoom in on the occupations of four consecutive extended-molecule states denoted in (a). An illustration of the corresponding molecular orbitals within the extended molecule region is shown in (c) and their effective couplings to the left (source) and right (sink) leads are given in (d). Adapted with permission from Ref. [120].

relatively large explicit lead models (see Figure 4), such that any memory effects within the leads decay at a time-scale that is much shorter than the dynamical time-scale of the active molecule of interest. Naturally, the larger the lead models are, the better the Markovian approximation becomes. Nonetheless, since one is forced to work with finite lead models, lead level broadening is introduced via Γ to obtain an effectively continuous spectrum. The sensitivity of the transport calculation results to the tradeoff between lead dimensions and level broadening has been extensively studied.[111,112,123–130] Specifically, a typical Kramer's turnover behavior has been demonstrated for many model systems with a broad parameter stability regime.[123,124,126–131] Figure 4 provides an example of the dependence of the steady-state current on the value of the driving rate for several tight-binding lead model sizes. For low driving rate values, the description of the equilibrium thermal distribution in the lead models is insufficient, resulting in an underestimated current (with respect to the reference Landauer value). Too high driving rate values provide a good description of the equilibrium state of the leads but given the finite number of modeled electrons this is done at the expense of current depletion in the molecule of interest. Fortunately, for sufficiently large lead models there is a large stability range, extending into the Markovian assumption validity region, where the DLvN steady-state current matches the Landauer reference value.

The above discussion demonstrates that meaningful current dynamics can be obtained using an appropriate choice of driving rate. While this can be achieved by tuning the driving rate to match the DLvN steady-state current to the Landauer reference value,[114,120,123,124,126–129] there is clearly an advantage to developing a parameter-free approach. This can be achieved by replacing the single driving rate, appearing as a fitting parameter in the original methodology, by a set of state-dependent broadening factors applied to the different single-particle lead levels.[132] These state-dependent broadening factors can be obtained explicitly by diagonalization of the lead Hamiltonian block, dressed by the self-energy matrix of the semi-infinite reservoir. This procedure is performed only once per reservoir model, and the obtained set of broadening factors is fully transferable to any molecular junction comprising the same leads. Figure 5 demonstrates the performance of this approach for a non-orthogonal basis-set representation of a hydrogen chain junction, where the obtained current dynamics matches that of the early micro-canonical current, and the emerging steady-state current matches the expected Landauer value, without being set to it by parameter tuning.

Going beyond the frozen nuclei picture, the DLvN was recently extended to address coupled electron-ion dynamics. Within the framework of the Born-Oppenheimer approximation in the adiabatic limit, it was demonstrated that when a molecule has a weak vibronic coupling in vacuum, steady-

Israel Journal of Chemistry

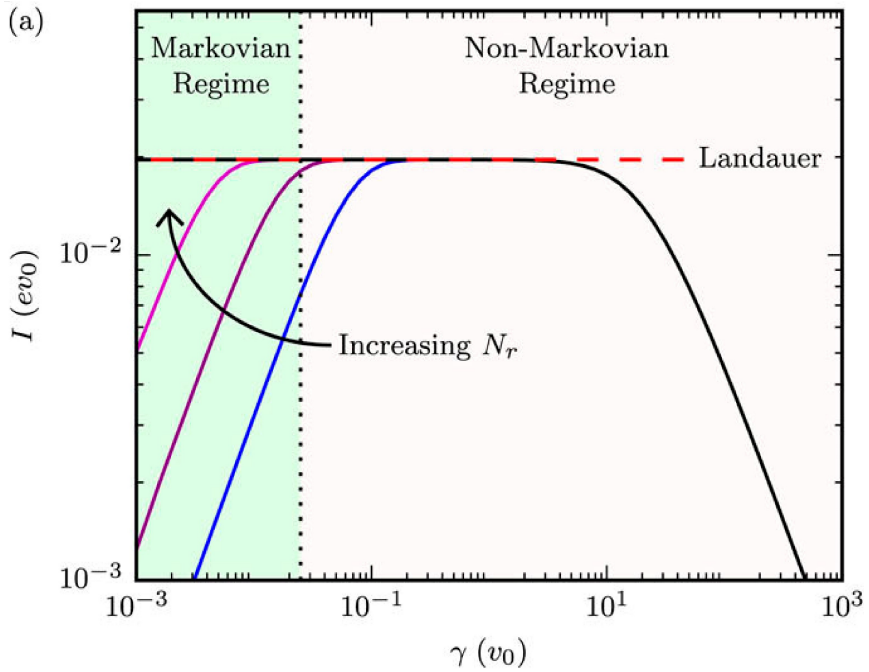

Figure 4. Steady-state current of a one-dimensional tight-binding junction model as a function of lead driving rate with an applied bias expressed as $V_{L(R)} = \pm v_0\hbar/4$, and an increasing number of explicit reservoir sites (32, 128, and 512). In the limit of an infinite number of explicit lead states, the plateau extends to $\gamma = 0$, yielding the Landauer/Meir-Wingreen current (red dashed line). The vertical dotted black line marks the region where the Markovian master equation is valid, which can be numerically reached by a sufficient increase of the number of reservoir sites. Adapted with permission from Ref. [124].

state current may not be achievable even for a very short molecular length and that molecular vibrations are manifested in the current fluctuations.[133] Furthermore, the approach reproduces qualitatively the Joule heating effect and predicts trends that are consistent with the microscopic version of Ohm's law, with some numerical deviations from Fermi's golden rule that remain to be addressed.[134]

Having established the DLvN methodology for simulating electron dynamics in open quantum systems, we now turn to discussing some of its recent applications. Within the realm of molecular electronics, molecular interferometry emerges as a promising direction for designing active components with unique functionalities. In this context, the DLvN approach was recently applied in conjunction with a magnetic extended Hückel Hamiltonian to study dynamical aspects of current switching in Aharonov-Bohm molecular rings.[135] Figure 6 presents an example of such switching upon the application of a magnetic field perpendicular to the surface of a symmetrically contacted hydrogen ring, corresponding to half the Aharonov-Bohm cycle. Snapshots of the charge density variations illustrate real-time interferometric effects.

Another promising research direction made available with the development of the DLvN approach is the numerical investigation of unexplored non-equilibrium thermodynamic phenomena in open quantum systems driven far from equilibrium. Analytical treatments of this problem provide important insights;[16,136–148] However, they typically rely on expansions in powers of the driving rate and are difficult to apply under fast driving or to strong system-bath coupling scenarios. The DLvN approach is free from this limitation, allowing the study of rapidly driven systems with arbitrary lead band structure.[149,150] This was recently demonstrated for the driven resonant level model, where the formal basis for evaluating thermodynamic observables from a DLvN simulation was provided and applied to the calculation of work, heat, and entropy variations at different driving rate regimes.[151–153]

The above applications exemplify the power of the DLvN approach to study quantum dynamical phenomena of open systems in unexplored regimes. Nonetheless, to unleash the full potential of the approach, it should be applied in conjunction with first-principles electronic structure treatments. Being based on effective single-particle Hamiltonians, the natural choice for DLvN would be time-dependent density functional theory, which provides formally exact dynamics within the framework of Kohn-Sham one-electron orbitals.[84] The first TDDFT implementation of the DLvN approach was introduced by Morzan et al.[154,155] In their approach, the site-to-state transformation was circumvented by using the ground state density matrix of the finite model junction under an axial electric field as a reference state. Avoiding the site-to-state transformation is clearly advantageous in terms of computational efficiency. However, it requires a modification of the equation of motion, adding

Israel Journal of Chemistry

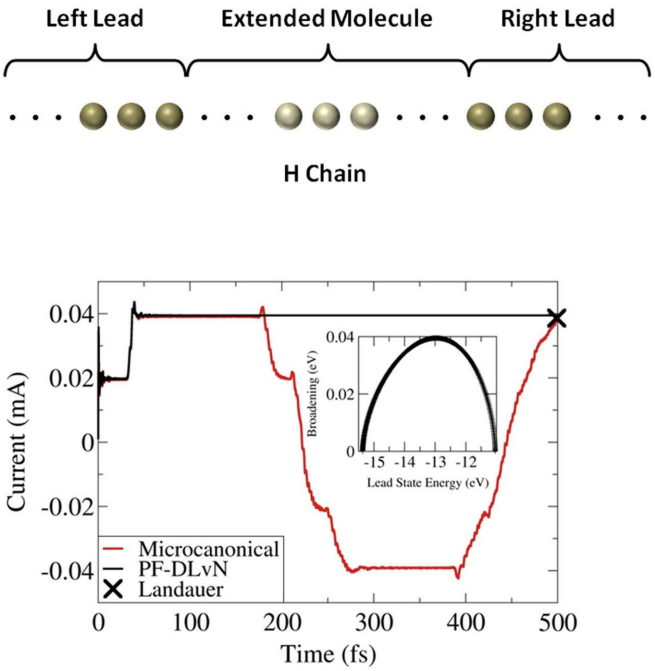

Figure 5. Application of the parameter free DLvN approach to an extended Hückel non-orthogonal basis-set representation of a hydrogen-based molecular junction model consisting of an equi-spaced (2Å) 110 atom extended-molecule chain bridging two 300 hydrogen atom chain lead models (upper panel). The lower panel presents the parameter-free DLvN (black line) and the microcanonical (red line) time-dependent currents at a bias voltage of 0.5 V and reservoir electronic temperatures of 0 K. The corresponding steady-state Landauer current is presented as reference by the X mark. Insets: lead state-dependent broadening factors calculated using the parameter-free DLvN methodology (black "+" marks). Adapted with permission from Ref. [132].

non-vanishing target coherence matrix blocks that can be traced to the Green's function-based "hairy-probes" method.[156,157] Furthermore, the alternative utilization of field-induced polarized boundary conditions compromises the appropriate representation of the equilibrium state of the reservoirs, as characterized by their respective Fermi-Dirac occupations,[158] and may lead to possible violations of Pauli's exclusion principle.[157] Additionally, approaches based on field-induced polarized boundary conditions are also practically limited to linear two-lead setups, where a uniform field is applied along the main axis of the junction model to define the initial reference state, whereas the original formalism is equally valid for multi-terminal setups.[114] Despite these limitations, the TDDFT implementation of the DLvN approach[154] provided an important step forward towards the accurate real-time simulation of electron dynamics in realistic molecular junctions. Furthermore, this approach has been extended to provide a TDDFT description of the molecule, embedded within a tight-binding description of the leads, resulting in a hybrid multiscale approach that can provide first-principles accuracy of the dynamics of interest at a considerably reduced computational cost.[155,159]

More recently, a spin-compensated TDDFT implementation of the DLvN approach that imposes open boundary conditions via the site-to-state transformation was presented.[160] While being more computationally demanding, it was found to conserve both Pauli's exclusion principle and density matrix positivity within a numerically stable scheme. First, the current dynamics of a simplified hydrogen chain model was investigated, demonstrating how current density variations can be explored using the developed approach (Figure 7). The method was then applied to a more realistic model junction, consisting of a benzene molecule bridging two graphene nanoribbon leads, demonstrating how the steady state emerges out of the initial transient dynamics under different bias voltages.

Summary and Outlook

In this article, we have presented a concise overview of the background, rationale, theoretical basis, formalism, extensions, and applications of the driven Liouville von Neumann methodology. This approach provides a physically motivated, computationally efficient, and formally sound framework for imposing non-equilibrium open boundary conditions on finite quantum model systems that can be described by effective single-particle Hamiltonians. In recent years, important advances have been made both in terms of understanding the formal foundation of the theory and its implementation, especially in conjunction with first-principles treatments and within multi-scale approaches. Further research opportunities await, not only in terms of novel applications, but also in terms of methodological development including, e.g., spin-uncompensated and non-collinear spin treatments, time-dependent bias and gate voltages, coupled electron-nuclear dynamics,[133,134,156,161–166] and much more. Opportunities also await in improvements of the numerical algorithms and their implementations in state-of-the-art computational platforms. A full-fledged first-principles implementation of the DLvN approach, accounting for all these effects, is expected to have broad impact on, e.g., the study of central problems in out-of-equilibrium quantum thermodynamics, the simulation of novel quantum computing setups, and the design of new molecular electronics and spintronics devices.

Acknowledgements

O.H. is grateful for the generous financial support of The Ministry of Science and Technology of Israel (Grant No. 3-16244), the Center for Nanoscience and Nanotechnology of Tel-Aviv University, and the Heineman Chair in Physical Chemistry. L.K. thanks the Aryeh and Mintzi Katzman Professorial Chair and the Helen and Martin Kimmel Award for Innovative Investigation.

Israel Journal of Chemistry

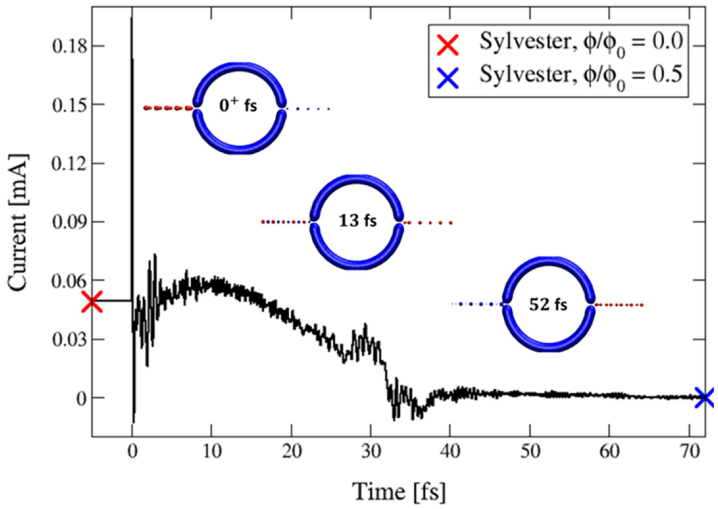

Figure 6. Current switching dynamics (obtained under a bias voltage of V) in a strongly coupled symmetric Aharonov-Bohm hydrogen ring, due to the application of magnetic fluxes corresponding to $\phi = 0.5\phi_0$ and $\phi \approx 0.2\phi_0$, respectively, where $\phi_0 = h/2e$ is the magnetic flux quantum. Snapshots of the variations in the electron density (with respect to the field-free steady-state density) during transient dynamics are shown in the insets at time frames of 0.01, 13, and 52 *fs* after switching on the magnetic field. Steady-state current values obtained using the Sylvester equation[112] in the absence and presence of the magnetic field are marked by the red and blue X marks, respectively. Adapted with permission from Ref. [135].

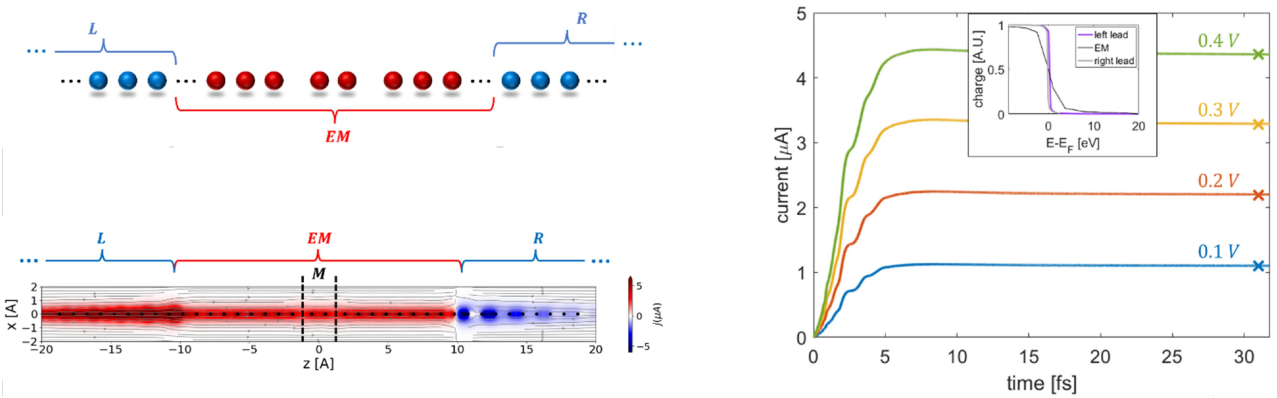

Figure 7. DLvN-TDDFT dynamical transport simulations of a hydrogen chain junction model. Top left: Real-space formal partition of a hydrogen chain junction model into left (L) and right (R) lead sections and an extended molecule (EM) region. Bottom left: Time-dependent current calculated at various bias voltages (0.1 (blue), 0.2 (orange), 0.3 (yellow), and 0.4 (green) V) for a 380 atom hydrogen chain with $N_M = 2$, $N_{EM} = 20$, and $N_{L/R} = 180$. The reservoir electronic temperatures are set to $T_L = T_R = 315.7$ K and the driving rate (see Eq. 9) used is $\hbar\Gamma = 0.61$ eV. The colored X marks designate the corresponding Sylvester[112] steady-state currents. Inset: left lead (purple), right lead (grey), and extended molecule (black) steady-state occupations obtained at $t = 25$ *fs* under a bias voltage of 0.2 *V*. Right: Spatially resolved steady-state current map of the hydrogen chain molecular junction model under a bias voltage of $V = 0.3$ *V*. The heat map represents the axial (z) current component, the streamlines represent the projection of the local current density vector on the x-z plane, and the black dots represent the position of the hydrogen atoms in the vicinity of the extended molecule section. The border lines between the extended molecule section and the source and sink driven leads are located at ±10.3 Å, and the seam lines between the weakly coupled molecule and the left and right segments of the *EM* are located at ±1.2 Å, as marked by the vertical black dashed lines. Adapted with permission from Ref. [160].

References

[1] A. Aviram, M. A. Ratner, *Chem. Phys. Lett.* **1974**, *29*, 277–283 .
[2] J. Jortner, M. A. Ratner, *Molecular Electronics, Blackwell Science Inc.* **1997**.
[3] N. S. Hush, *Annals of the New York Academy of Sciences* **2003**, *1006*, 1–20.
[4] J. R. Heath, M. A. Ratner, *Physics Today* **2003**, *56*, 43–49.
[5] Y. Selzer, D. L. Allara, *Annu. Rev. Phys. Chem.* **2006**, *57*, 593–623.
[6] J. R. Heath, *Annu. Rev. Mater. Res.* **2009**, *39*, 1–23.
[7] J. C. Cuevas, E. Scheer, *Molecular Electronics: An Introduction to Theory and Experiment, 1st Edition*, World Scientific, **2010**.

[8] I. Baldea, *Molecular Electronics: An Experimental and Theoretical Approach, 1st Edition*, Stanford Publishing, **2015**.
[9] D. Xiang, X. Wang, C. Jia, T. Lee, X. Guo, *Chem. Rev.* **2016**, *116*, 4318–4440.
[10] N. Xin, et al., *Nat. Rev. Phys.* **2019**, *1*, 211–230.
[11] H. Chen, J. Fraser Stoddart, *Nat. Rev. Mater.* **2021**, *6*, 804–828.
[12] G. A. Prinz, *Physics Today* **1995**, *48*, 58–63.
[13] S. A. Wolf, et al., *Science* **2001**, *294*, 1488–1495.
[14] A. Nitzan, M. A. Ratner, *Science* **2003**, *300*, 1384–1389.
[15] I. Žutić, J. Fabian, S. Das Sarma, *Rev. Mod. Phys.* **2004**, *76*, 323–410.
[16] M. Esposito, M. A. Ochoa, M. Galperin, *Phys. Rev. Lett.* **2015**, *114*, 080602.
[17] R. Alicki, R. Kosloff, in *Thermodynamics in the Quantum Regime: Fundamental Aspects and New Directions* (Eds.: F. Binder *et al.*) Springer International Publishing, **2018**, pp. 1–33.
[18] R. Kosloff, *J. Chem. Phys.* **2019**, *150*, 204105.
[19] W. Dou, J. Bätge, A. Levy, M. Thoss, *Phys. Rev. B* **2020**, *101*, 184304.
[20] N. Bergmann, M. Galperin, *Eur. Phys. J. Spec. Top.* **2021**, *230*, 859–866.
[21] A. Grimaldi, A. Sergi, A. Messina, *Entropy* **2021**, *23*, 147.
[22] R. Landauer, *IBM J. Res. Dev.* **1957**, *1*, 223.
[23] M. Büttiker, *Phys. Rev. Lett.* **1986**, *57*, 1761–1764.
[24] S. Datta, *Electronic Transport in Mesoscopic Systems*, Cambridge University Press, **1995**.
[25] Y. Imry, R. Landauer, *Rev. Mod. Phys.* **1999**, *71*, S306–S312.
[26] Y. Imry, *Introduction to Mesoscopic Physics.* 2nd Edition, Oxford University Press, **2002**.
[27] M. Di Ventra, *Electrical Transport in Nanoscale Systems, 1st Edition*, Cambridge University Press, **2008**.
[28] G. Cuniberti, G. Fagas, K. Richter, *Introducing Molecular Electronics, Lecture Notes in Physics*, Springer Verlag, **2005**.
[29] C. Caroli, R. Combescot, P. Nozieres, D. Saint-James, *J. Phys. C Solid State Phys.* **1971**, *4*, 916.
[30] C. Caroli, R. Combescot, D. Lederer, P. Nozieres, D. Saint-James, *J. Phys. C: Solid State Phys.* **1971**, *4*, 2598.
[31] Y. Meir, N. S. Wingreen, *Phys. Rev. Lett.* **1992**, *68*, 2512–2515.
[32] M. Cini, *Phys. Rev. B* **1980**, *22*, 5887–5899.
[33] P. Delaney, J. C. Greer, *Phys. Rev. Lett.* **2004**, *93*, 036805.
[34] G. Fagas, P. Delaney, J. C. Greer, *Phys. Rev. B* **2006**, *73*, 241314.
[35] N. D. Lang, *Phys. Rev. B* **1995**, *52*, 5335–5342.
[36] P. A. Derosa, J. M. Seminario, *J. Phys. Chem. B* **2000**, *105*, 471–481.
[37] J. Taylor, H. Guo, J. Wang, *Phys. Rev. B* **2001**, *63*, 245407.
[38] M. Brandbyge, J.-L. Mozos, P. Ordejón, J. Taylor, K. Stokbro, *Phys. Rev. B* **2002**, *65*, 165401.
[39] Y. Xue, S. Datta, M. A Ratner, *Chem. Phys.* **2002**, *281*, 151–170.
[40] J. J. Palacios, A. J. Pérez-Jiménez, E. Louis, E. SanFabián, J. A. Vergés, *Phys. Rev. B* **2002**, *66*, 035322.
[41] A. Calzolari, N. Marzari, I. Souza, M. Buongiorno Nardelli, *Phys. Rev. B* **2004**, *69*, 035108.
[42] O. Hod, J. E. Peralta, G. E. Scuseria, *J. Chem. Phys.* **2006**, *125*, 114704.
[43] J. Jiang, M. Kula, Y. Luo, *J. Chem. Phys.* **2006**, *124*, 034708–034710.
[44] F. Evers, F. Weigend, M. Koentopp, *Phys. Rev. B* **2004**, *69*, 235411.
[45] K. H. Khoo, J. B. Neaton, H. J. Choi, S. G. Louie, *Phys. Rev. B* **2008**, *77*, 115326.
[46] S. T. Pantelides, M. Di Ventra, N. D. Lang, *Phys. Rev. B* **2001**, *296*, 72–77.
[47] K. Burke, R. Car, R. Gebauer, *Phys. Rev. Lett.* **2005**, *94*, 146803.
[48] M. Koentopp, C. Chang, K. Burke, R. Car, *J. Phys.: Condens. Matter* **2008**, *20*, 083203.
[49] P. S. Krstić, et al., *Comput. Mater. Sci.* **2003**, *28*, 321–341.
[50] S. Y. Quek, et al., *Nano Lett.* **2007**, *7*, 3477–3482.
[51] R. Baer, D. Neuhauser, *Int. J. Quantum Chem.* **2003**, *91*, 524–532.
[52] R. Baer, T. Seideman, S. Ilani, D. Neuhauser, *J. Chem. Phys.* **2004**, *120*, 3387–3396 .
[53] G. Stefanucci, C.-O. Almbladh, *Europhys. Lett.* **2004**, *67*, 14–20.
[54] G. Stefanucci, C.-O. Almbladh, *Phys. Rev. B* **2004**, *69*, 195318.
[55] M. Di Ventra, T. N. Todorov, *J. Phys.: Condens. Matter* **2004**, *16*, 8025–8034 .
[56] S. Kurth, G. Stefanucci, C. O. Almbladh, A. Rubio, E. K. U. Gross, *Phys. Rev. B* **2005**, *72*, 035308.
[57] N. Bushong, N. Sai, M. Di Ventra, *Nano Lett.* **2005**, *5*, 2569–2572.
[58] G. Stefanucci, C.-O. Almbladh, *J. Phys.: Conf. Ser.* **2006**, *35*, 17.
[59] G. Stefanucci, et al., *Lecture Notes in Physics*, Vol. 706 (Eds Miguel Marques *et al.*), Springer Berlin/Heidelberg, **2006**, 479–492.
[60] R. D'Agosta, M. D. Ventra, *Journal of Physics: Condensed Matter* **2006**, *18*, 11059.
[61] J. Maciejko, J. Wang, H. Guo, *Phys. Rev. B* **2006**, *74*, 085324.
[62] M. Di Ventra, R. D'Agosta, *Phys. Rev. Lett.* **2007**, *98*, 226403.
[63] N. Bushong, J. Gamble, M. Di Ventra, *Nano Lett.* **2007**, *7*, 1789–1792.
[64] N. Sai, N. Bushong, R. Hatcher, M. Di Ventra, *Phys. Rev. B* **2007**, *75*, 115410.
[65] X.-Q. Li, Y. Yan, *Phys. Rev. B* **2007**, *75*, 075114.
[66] G. Stefanucci, *Phys. Rev. B* **2007**, *75*, 195115.
[67] M. Galperin, S. Tretiak, *J. Chem. Phys.* **2008**, *128*, 124705.
[68] E. Khosravi, S. Kurth, G. Stefanucci, E. Gross, *Appl. Phys. A* **2008**, *93*, 355–364.
[69] R. D'Agosta, M. Di Ventra, *Phys. Rev. B* **2008**, *78*, 165105.
[70] A. Prociuk, B. D. Dunietz, *Phys. Rev. B* **2008**, *78*, 165112.
[71] G. Stefanucci, S. Kurth, A. Rubio, E. K. U. Gross, *Phys. Rev. B* **2008**, *77*, 075339.
[72] X. Zheng, G. Chen, *Lecture Notes in Nanoscale Science and Technology*, Vol. 2 (eds Zikang Tang & Ping Sheng), Springer New York, **2008**, 235–243.
[73] J. S. Evans, T. van Voorhis, *Nano Lett.* **2009**, *9*, 2671–2675.
[74] J. Yuen-Zhou, C. Rodriguez-Rosario, A. Aspuru-Guzik, *Phys. Chem. Chem. Phys.* **2009**, *11*, 4509–4522.
[75] Z. Zhou, S.-I. Chu, *Europhys. Lett.* **2009**, *88*, 17008.
[76] P. Myöhänen, A. Stan, G. Stefanucci, R. van Leeuwen, *Phys. Rev. B* **2009**, *80*, 115107.
[77] J. Yuen-Zhou, D. G. Tempel, C. A. Rodríguez-Rosario, A. Aspuru-Guzik, *Phys. Rev. Lett.* **2010**, *104*, 043001.
[78] X. Zheng, et al., *J. Chem. Phys.* **2010**, *133*, 114101.
[79] S. Ke, R. Liu, W. Yang, H. U. Baranger, *J. Chem. Phys.* **2010**, *132*, 234105.
[80] D. G. Tempel, *J. Chem. Phys.* **2011**, *134*, 074116.
[81] G. Cohen, E. Gull, D. R. Reichman, A. J. Millis, *Phys. Rev. Lett.* **2015**, *115*, 266802.
[82] H. Cao, M. Zhang, T. Tao, M. Song, C. Zhang, *J. Chem. Phys.* **2015**, *142*, 084705.
[83] P. Schaffhauser, S. Kümmel, *Phys. Rev. B* **2016**, *93*, 035115.
[84] S. Kurth, G. Stefanucci, *J. Phys. Condens. Matter* **2017**, *29*, 413002.
[85] M. Galperin, *Chem. Soc. Rev.* **2017**, *46*, 4000–4019.

[86] H. Rahman, U. Kleinekathöfer, *J. Chem. Phys.* **2018**, *149*, 234108.
[87] M. Ridley, E. Gull, G. Cohen, *J. Chem. Phys.* **2019**, *150*, 244107.
[88] M. Ridley, N. W. Talarico, D. Karlsson, N. Lo Gullo, R. Tuovinen, *J. Phys. A Math. Theor.* **2022**, *55*, 273001.
[89] W. R. Frensley, *Rev. Mod. Phys.* **1990**, *62*, 745–791.
[90] X. Zheng, F. Wang, C. Y. Yam, Y. Mo, G. Chen, *Phys. Rev. B* **2007**, *75*, 195127.
[91] Y. Wang, C. Y. Yam, T. Frauenheim, G. H. Chen, T. A. Niehaus, *Chem. Phys.* **2011**, *391*, 69–77.
[92] S. K. Koo, C. Y. Yam, X. Zheng, G. Chen, *Phys. Status Solidi B* **2012**, *249*, 270–275.
[93] S. Chen, Y. Kwok, G. Chen, *Acc. Chem. Res.* **2018**, *51*, 385–393.
[94] R. M. Martin, *Electronic Structure: Basic Theory and Practical Methods*, Cambridge University Press, **2004**.
[95] C.-L. Cheng, J. S. Evans, T. van Voorhis, *Phys. Rev. B* **2006**, *74*, 155112.
[96] l. Ercan, N. G. Anderson, *J. Appl. Phys.* **2010**, *107*, 124318.
[97] R. Gebauer, R. Car, *Int. J. Quantum Chem.* **2005**, *101*, 564–571.
[98] A. Bodor, L. Diósi, *Phys. Rev. A* **2006**, *73*, 064101.
[99] R. Gebauer, K. Burke, R. Car, *Lecture Notes in Physics*, Vol. 706 (eds Miguel Marques et al.), Springer Berlin/Heidelberg, **2006**, 463–477.
[100] R. Gebauer, S. Piccinin, R. Car, *ChemPhysChem* **2005**, *6*, 1727–1730.
[101] T. M. Henderson, G. Fagas, E. Hyde, J. C. Greer, *J. Chem. Phys.* **2006**, *125*, 244104.
[102] O. Hod, E. Rabani, R. Baer, *Acc. Chem. Res.* **2005**, *39*, 109–117.
[103] O. Hod, R. Baer, E. Rabani, *J. Am. Chem. Soc.* **2005**, *127*, 1648–1649.
[104] O. Hod, R. Baer, E. Rabani, *J. Phys: Condens. Matter* **2008**, *20*, 383201.
[105] J. A. Driscoll, K. Varga, *Phys. Rev. B* **2008**, *78*, 245118.
[106] K. Varga, *Phys. Stat. Sol. B* **2009**, *246*, 1407–1412.
[107] B. G. Cook, P. Dignard, K. Varga, *Phys. Rev. B* **2011**, *83*, 205105.
[108] L. Zhang, J. Chen, J. Wang, *Phys. Rev. B* **2013**, *87*, 205401.
[109] H. Xie, Y. Kwok, F. Jiang, X. Zheng, G. Chen, *J. Chem. Phys.* **2014**, *141*, 164122.
[110] A. P. Horsfield, D. R. Bowler, A. J. Fisher, *J. Phys.: Condens. Matter* **2004**, *16*, L65.
[111] C. G. Sánchez, *et al. J. Chem. Phys.* **2006**, *124*, 214708.
[112] J. E. Subotnik, T. Hansen, M. A. Ratner, A. Nitzan, *J. Chem. Phys.* **2009**, *130*, 144105.
[113] A. E. Rothman, D. A. Mazziotti, *J. Chem. Phys.* **2010**, *132*, 104112.
[114] T. Zelovich, L. Kronik, O. Hod, *J. Chem. Theor. Comput.* **2014**, *10*, 2927–2941.
[115] T. Zelovich, L. Kronik, O. Hod, *J. Chem. Theory and Comput.* **2015**, *11*, 4861–4869.
[116] T. Zelovich, T. Hansen, M. E. Tuckerman, *Nano Lett.* **2022**, *22*, 9854–9860.
[117] L. Chen, T. Hansen, I. Franco, *J. Phys. Chem. C* **2014**, *118*, 20009–20017.
[118] O. Hod, C. A. Rodríguez-Rosario, T. Zelovich, T. Frauenheim, *J. Phys. Chem. A* **2016**, *120*, 3278–3285.
[119] V. Pohl, L. E. Marsoner Steinkasserer, J. C. Tremblay, *J. Phys. Chem. Lett.* **2019**, *10*, 5387–5394.
[120] T. Zelovich, L. Kronik, O. Hod, *J. Phys. Chem. C* **2016**, *120*, 15052–15062.
[121] Y. H. Kwok, H. Xie, C. Y. Yam, X. Zheng, G. H. Chen, *J. Chem. Phys.* **2013**, *139*.
[122] A. Nitzan, *Chemical Dynamics in Condensed Phases: Relaxation, Transfer and Reactions in Condensed Molecular Systems*, Oxford University Press, **2006**.
[123] D. Gruss, K. A. Velizhanin, M. Zwolak, *Sci. Rep.* **2016**, *6*, 24514.
[124] J. E. Elenewski, D. Gruss, M. Zwolak, *J. Chem. Phys.* **2017**, *147*, 151101.
[125] W. Chu, X. Li, *J. Chem. Theory Comput.* **2020**, *16*, 3746–3756.
[126] G. Wójtowicz, J. E. Elenewski, M. M. Rams, M. Zwolak, *Phys. Rev. A* **2020**, *101*, 050301.
[127] T.-M. Chiang, L.-Y. Hsu, *J. Chem. Phys.* **2020**, *153*, 044103.
[128] G. Wójtowicz, J. E. Elenewski, M. M. Rams, M. Zwolak, *Phys. Rev. B* **2021**, *104*, 165131.
[129] J. E. Elenewski, G. Wójtowicz, M. M. Rams, M. Zwolak, *J. Chem. Phys.* **2021**, *155*, 124117.
[130] B. De, G. Wojtowicz, J. Zakrzewski, M. Zwolak, M. M. Rams, https://doi.org/10.48550/arXiv.2303.04160, **2023**.
[131] G. Wójtowicz, A. Purkayastha, M. Zwolak, M. M. Rams, *Phys. Rev. B* **2023**, *107*, 035150.
[132] T. Zelovich, et al., *J. Chem. Phys.* **2017**, *146*, 092331.
[133] T.-M. Chiang, Q.-R. Huang, L.-Y. Hsu, *J. Phys. Chem. C* **2019**, *123*, 10746–10755.
[134] C. M. Bustamante, T. N. Todorov, C. G. Sánchez, A. Horsfield, D. A. Scherlis, *J. Chem. Phys.* **2020**, *153*, 234108.
[135] T. Maaravi, O. Hod, *J. Phys. Chem. C* **2020**, *124*, 8652–8662.
[136] L. Arrachea, E. R. Mucciolo, C. Chamon, R. B. Capaz, *Phys. Rev. B* **2012**, *86*, 125424.
[137] R. Kosloff, A. Levy, *Annu. Rev. Phys. Chem.* **2014**, *65*, 365–393.
[138] M. F. Ludovico, J. S. Lim, M. Moskalets, L. Arrachea, D. Sánchez, *Phys. Rev. B* **2014**, *89*, 161306.
[139] D. Gelbwaser-Klimovsky, W. Niedenzu, G. Kurizki, in *Advances In Atomic, Molecular, and Optical Physics* Vol. 64 (eds Ennio Arimondo, Chun C. Lin, & Susanne F. Yelin), Academic Press, **2015**, 329–407.
[140] A. Bruch, M. Thomas, S. V. Kusminskiy, F. von Oppen, A. Nitzan, *Phys. Rev. B* **2016**, *93*, 115318.
[141] M. F. Ludovico, M. Moskalets, D. Sánchez, L. Arrachea, *Phys. Rev. B* **2016**, *94*, 035436.
[142] R. Tuovinen, N. Säkkinen, D. Karlsson, G. Stefanucci, R. van Leeuwen, *Phys. Rev. B* **2016**, *93*, 214301.
[143] M. A. Ochoa, A. Bruch, A. Nitzan, *Phys. Rev. B* **2016**, *94*, 035420.
[144] V. Cavina, A. Mari, V. Giovannetti, *Phys. Rev. Lett.* **2017**, *119*, 050601.
[145] J. Thingna, F. Barra, M. Esposito, *Phys. Rev. E* **2017**, *96*, 052132.
[146] V. Cavina, A. Mari, A. Carlini, V. Giovannetti, *Phys. Rev. A* **2018**, *98*, 012139.
[147] M. A. Ochoa, N. Zimbovskaya, A. Nitzan, *Phys. Rev. B* **2018**, *97*, 085434.
[148] W. Dou, M. A. Ochoa, A. Nitzan, J. E. Subotnik, *Phys. Rev. B* **2018**, *98*, 134306.
[149] A. M. Lacerda, A. Purkayastha, M. Kewming, G. T. Landi, J. Goold, https://doi.org/10.48550/arXiv.2206.01090, **2022**.
[150] M. Brenes, et al. https://doi.org/10.48550/arXiv.2211.13832, **2022**.
[151] I. Oz, O. Hod, A. Nitzan, *Mol. Phys.* **2019**, *117*, 2083–2096.
[152] A. Oz, O. Hod, A. Nitzan, *J. Chem. Theory and Comput.* **2020**, *16*, 1232–1248.
[153] J. Liu, K. A. Jung, D. Segal, *Phys. Rev. Lett.* **2021**, *127*, 200602.

[154] U. N. Morzan, F. F. Ramírez, M. C. G. Lebrero, D. A. Scherlis, *J. Chem. Phys.* **2017**, *146*, 044110.
[155] C. M. Bustamante, F. F. Ramírez, C. G. Sánchez, D. A. Scherlis, *J. Chem. Phys.* **2019**, *151*, 084105.
[156] E. J. McEniry, et al., *J. Phys.: Condens. Matter* **2007**, *19*, 196201.
[157] F. Ramírez, D. Dundas, C. G. Sánchez, D. A. Scherlis, T. N. Todorov, *J. Phys. Chem. C* **2019**, *123*, 12542–12555.
[158] T. S. Nguyen, R. Nanguneri, J. Parkhill, *J. Chem. Phys.* **2015**, *142*, 134113.
[159] F. F. Ramirez, C. M. Bustamente, M. C. González Lebrero, D. A. Scherlis, *J. Chem. Theory Comput.* **2020**, *16*, 2930–2940.
[160] A. Oz, A. Nitzan, O. Hod, J. E. Peralta, https://doi.org/10.48550/arXiv.2305.04343 (2023).
[161] R. E. Allen, *Phys. Rev. B* **1994**, *50*, 18629–18632.
[162] M. Galperin, M. A. Ratner, A. Nitzan, *J. Chem. Phys.* **2004**, *121*, 11965–11979.
[163] D. R. Bowler, A. P. Horsfield, C. G. Sánchez, T. N. Todorov, *J. Phys.: Condens. Matter* **2005**, *17*, 3985.
[164] C. Verdozzi, G. Stefanucci, C.-O. Almbladh, *Phys. Rev. Lett.* **2006**, *97*, 046603.
[165] J. Jakowski, K. Morokuma, *J. Chem. Phys.* **2009**, *130*, 224106.
[166] M. Todorović, D. R. Bowler, *J. Phys.: Condens. Matter* **2011**, *23*, 345301.

Manuscript received: March 29, 2023
Version of record online: May 10, 2023